GCU
Glasgow Caledonian University

University for the Common Good

On-line Monitoring and Analysis of the Dielectric Loss in Cross-bonded HV Cable system

Yang Yang[1]*, Donald M. Hepburn[1], Chengke Zhou[1], Wenjun Zhou[2], Yuchuan Bao[3] and Zhi Tian[3]
1 School of Engineering and Built Environment, Glasgow Caledonian University, Glasgow, UK, G4 0BA
2 School of Electrical Engineering, Wuhan University, Wuhan, China, 430072
3 Wuhan Power Supply Company, China State Grid, Wuhan, China, 430022
*Corresponding author (Tel.: +0044-747-771-2999; Email: yang.yang@gcu.ac.uk)

Abstract

Dielectric loss has long been recognized as one of the most important indicators of cable insulation health. Although huge efforts have been made in the past to measure the dielectric loss of cable circuits, there has been no report of any successful on-line techniques for the purpose. This paper proposes a new on-line insulation dielectric loss monitoring method, based on separation of currents collected from the co-axial cables connecting the cable sheaths and the cable link boxes. The principle and theoretical foundation of the method are demonstrated. MATLAB simulations, based on the real cable parameters in a 110 kV cable tunnel in China, indicate the error of the proposed method is less than 1×10^{-3} %. The criteria for determining the relative dielectric loss in cable segments, based on the leakage current separation results, are demonstrated at the end. Initial results and analysis of implementation of the proposed method in the real world 110 kV cable tunnel are presented.

Keywords: on-line monitoring; leakage current; dielectric loss; XLPE; cross bonding; three-phase

1. Introduction

Cross-bonded high voltage cable systems are widely adopted for long-distance power transmission and distribution in urban networks. Typical cross-bonded cable systems are usually implemented in major sections. Each major section has 9 cross-bonded minor sections. In comparison with single-end-grounded cable systems or both-end-grounded cable systems, a cross-bonded cable system is grounded at both ends of major section with cross bonding or interconnection of the minor cable section sheaths of the three phases to reduce or eliminate the effect of the induced voltage in the sheath and to reduce the sheath circulating currents.

However, the interconnection of the sheath creates differences between the on-line insulation monitoring methodology used in short-distance and long-distance power cables. Conventional off-line measurements utilize bridge methods to calculate the dielectric loss (DL) factor values [3] or phase difference between operating voltage vector and leakage current vector to compute DL factor. However, these methods have several drawbacks and cannot be applied in on-line monitoring. Firstly, under cross-bonding connection, sheath currents are a combination of the leakage currents from different minor sections and the unbalanced circulating current [7]. The unbalanced circulating currents result from differences in section lengths, unbalanced laying and unbalanced load currents [8]. Consequently, it is hard to detect the pure leakage current of each minor section for the calculation of DL angle. Secondly, for ease of installation and to avoid moisture intrusion, co-axial link cables are used for connecting the sheaths from joints to link boxes [1]. But this results in the current sensor clamped on the co-axial link cables detecting the vector sum of two sheath currents. Finally, for safety and operational reasons, it is usually difficult to detect the operational voltage directly at the terminals or joints. In addition, the voltage signals from the potential transformer (PT) in substations are usually not the same as the voltages at the terminals or joints [9]. And it is hard to quantify the difference.

Bing Pang and et al. in article [5] proposed an on-line DL factor monitoring method to determine the faults in minor sections of a major cross-bonded cable section. The method required acquisition of

voltage signals. As mentioned above, it is difficult to obtain when the cable circuit is in operation.

Massimo Marzinotto and et al. in article [6] proposed on-line measurement of the sheath-to-ground current to detect cable sheath faults. Although this offers the possibility of detecting sheath faults in a cross-bonded cable system, it cannot reflect the insulation conditions.

Consequently, a new method to address these issues is proposed in this paper by measuring the current at the co-axial cables to determine the relative dielectric loss. In the cross-bonded major section, 12 clamp-type current sensors are installed at the co-axial link cables. The proposed Leakage Current Separation Method (LCSM) aims at distinguishing the leakage currents from the sheath currents based on the 12 detected currents. The purpose of relative DL among three phases, based on the results of LCSM, is used to determine the relative insulation condition without acquiring the operational voltage signals.

The remainder of the paper is organized as follows

In Section 2, the theoretical background of the cross-bonded cable system connections and the currents in the sheath are introduced. In Section 3, the proposed Leakage Current Separation Method to differentiate leakage currents from sheath currents is explored by MATLAB simulations. In Section 4, the diagnosis of relative DL among three phases based on the results from LCSM is presented. In addition, a set of knowledge rules are given. In Section 5, a case study is discussed by analysing the on-line monitoring data from a 110 kV cross-bonded cable installed in a cable tunnel in China. In Section 6, the conclusions and the limitations are discussed.

2. Typical cross-bonded major section

2.1 The structure of the cross-bonded cable system investigated

Long distance power transmission by high voltage (HV) cables usually utilizes the series connection of several cross-bonded major sections. A typical cross-bonded major section is presented in Fig. 1 [4].
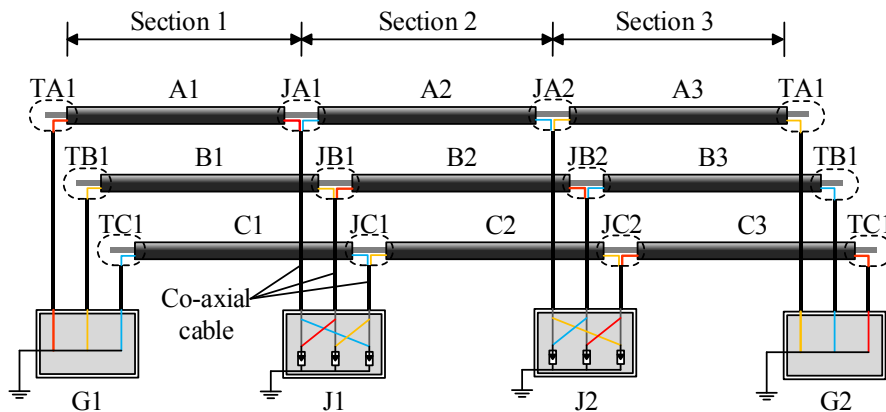

Fig. 1. A typical major section of a cross-bonded cable system

In Fig. 1, the major section consists of 9 minor sections named as A1, A2, A3, B1, B2, B3, C1, C2 and C3 in this work. The core conductor of a phase is connected contiguously, e.g. phase A runs through sections A1, A2 and A3. The sheaths of minor sections are cross-connected at cable joints, i.e. JA1, JB1, JC1, JA2, JB2 and JC2. The co-axial link cables connect the metal sheaths to the link boxes. The interconnections of the sheaths are implemented inside the link boxes, J1 and J2. The metal sheaths at both ends of a major section are directly connected to ground in the grounding boxes, G1 and G2.

Fig. 2 shows a typical link box with co-axial cable connections applied in the cross-bonded sheath

connection. In many parts of China, co-axial cables are used to bring the metal sheath conductors to the link boxes for ease of installation. Considering link box J1 from Fig.1, as indicated in Fig. 2, the sheath of A1 is connected to that of B2; B1 is connected to C2; C1 is connected to A2. Similarly, in link box J2 the connections would be: A2 connects to B3; B2 connects to C3; C2 connects to A3. Under normal conditions, when the voltages across the Over-Voltage Limiters (OVLs) are less than 50 V, the conductor clips in each link box are open-circuited. As a result, the sheath connections would be A1-B2-C3 (loop 1), B1-C2-A3 (loop 2) and C1-A2-B3 (loop 3). A simplified diagram of the cross-bonded sheath connection is shown in Fig. 3.
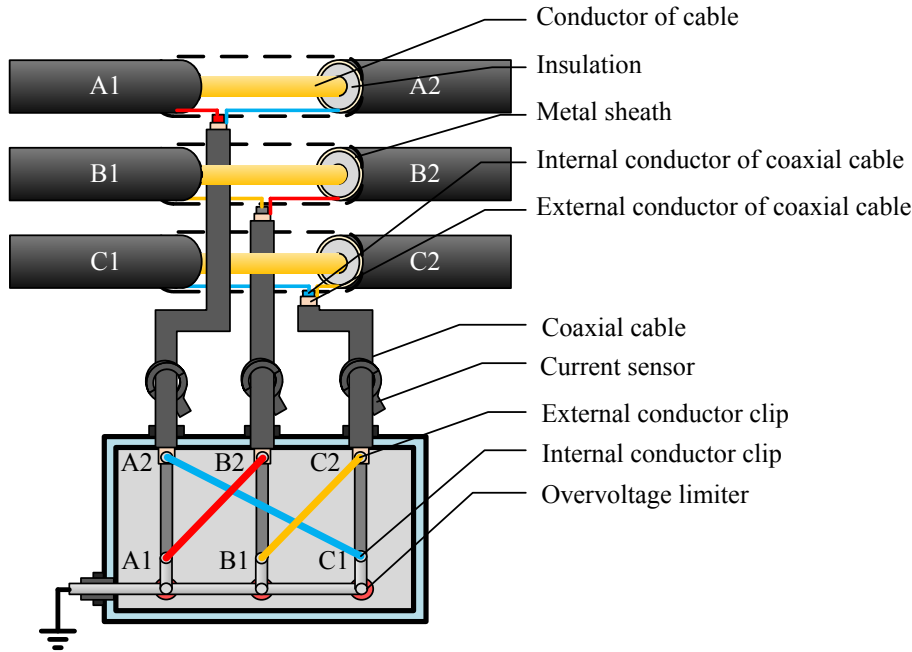
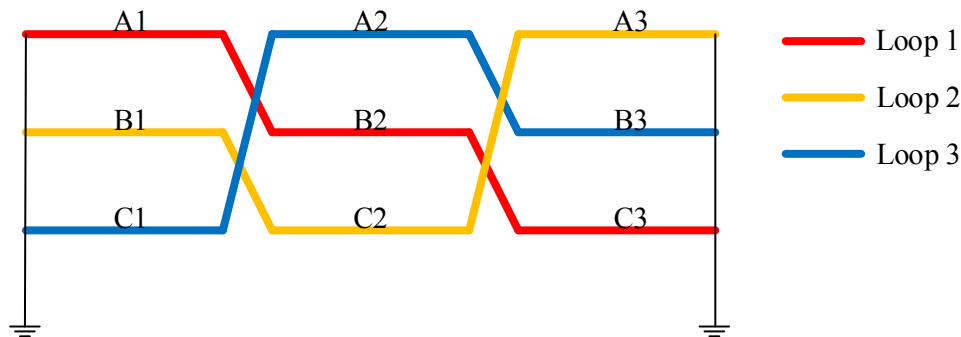Fig. 2. A typical link box with co-axial cables connection

Fig. 3. The simplified cross-bonded sheath connections

2.2. Leakage currents

In typical cross-bonded cable systems, both ends of the metal sheath in a major section are grounded, as shown schematically in Fig 4(a). Subsequently, the leakage current would split into two components flowing to both directions in the metal sheath, as red arrows move. Fig 4(b) shows the lumped circuit model. U_X is the operational voltage in the core conductor in phase X (where, X stands for the symbol of a phase, i.e., A, B or C); I_{Xn} is the leakage current through the insulation of minor section Xn (n = 1, 2, 3); C_{Xn} is the equivalent insulation capacitance in the minor section Xn; R_{Xn} is the equivalent insulation

3

resistance in the minor section Xn. $\mathbf{Z}_{mLXn}$ is the equivalent metal sheath impedance towards the power supply side, while $\mathbf{Z}_{mRXn}$ is the equivalent metal sheath impedance towards the load side. $\mathbf{I}_{LXn}$ is the leakage current component flowing to the earthing point at the power supply side; $\mathbf{I}_{RXn}$ is the leakage current component flowing to the earthing point near the load side.

(a) Leakage current distributed paths (red arrows)

(b) Lumped circuit for leakage current flowing through the minor section Xn
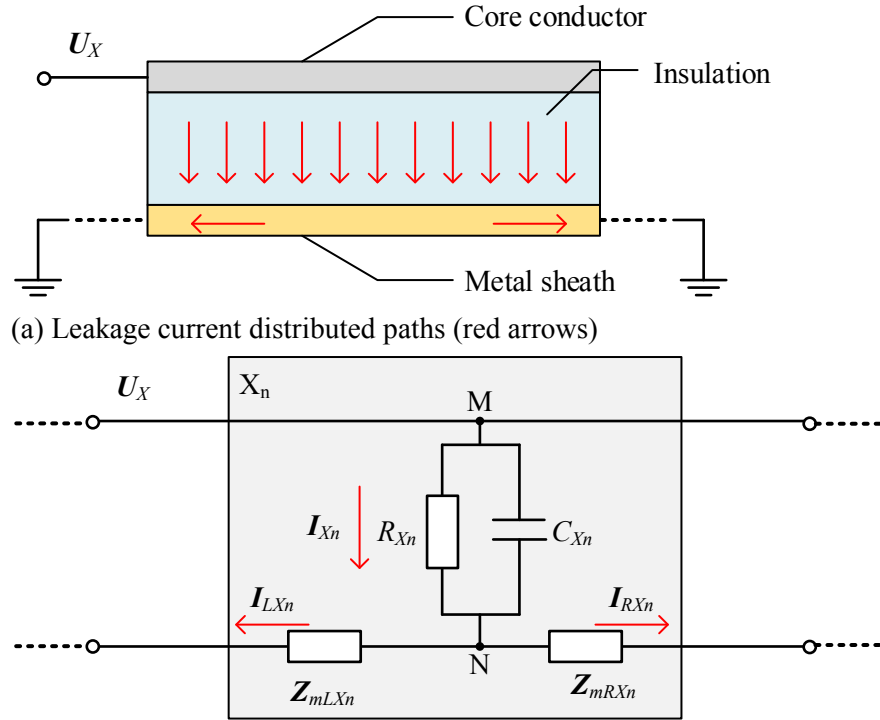
Fig. 4. Leakage current paths and model for an XLPE insulated minor section

Fig. 4(b) indicates that the vector sum of the leakage current components, $\mathbf{I}_{LXn}$ and $\mathbf{I}_{RXn}$, is equal to the leakage current vector of minor section Xn, as presented in Equation (1).

$$\mathbf{I}_{Xn} = \mathbf{I}_{LXn} + \mathbf{I}_{RXn} \tag{1}$$

2.3. Circulating currents

The HV cross-bonded cable system is grounded at both ends of each major section for safety reasons. However, it creates the loops for circulating currents. When the vector sum of induced voltages, such as $\mathbf{u}_{SA1}$, $\mathbf{u}_{SB2}$ and $\mathbf{u}_{SC3}$ in metal sheath loop 1, are not zero, due to unbalanced section lengths or unbalanced installation type, there will be circulating current, $\mathbf{I}_{m1}$, as shown in Fig. 5.
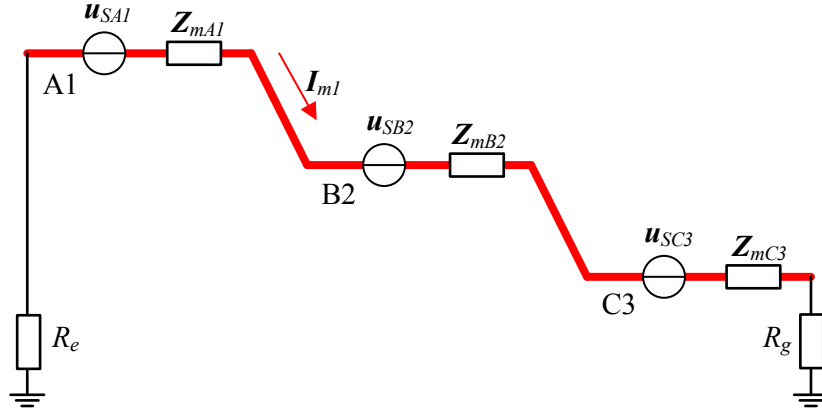
Fig. 5. The equivalent circuit of circulating current in sheath loop 1

The equations for the initial circulating currents shown in Fig. 5 are presented in Equation (2).

$$I_{m1} = \frac{u_{SA1} + u_{SB2} + u_{SC3}}{Z_{mA1} + Z_{mB2} + Z_{mC3} + R_e + R_g} \tag{2}$$

Where, u_{SXn} is the induced voltage in the sheath of the minor section Xn (X stands for A, B or C; n=1, 2, 3). This representation is also suitable for other two sheath loops.

As indicated in Equation (2), the circulating current is mainly dependent on the induced voltages in metal sheath and the impedances of the sheath loop. In addition, induced voltages are subject to the configuration of the major cable section, load currents and installation type. For a defined layout of a cross-bonded cable system, induced voltages in sheaths are mainly influenced by load currents.

2.4. Sheath currents

As presented in *Sections 2.2* and *2.3*, the sheath current is composed of leakage currents and circulating currents. Based on Fig. 1, Fig. 4 and Fig. 5, the superimposed currents in the simplified cross-bonded sheath system are presented in Fig. 6.
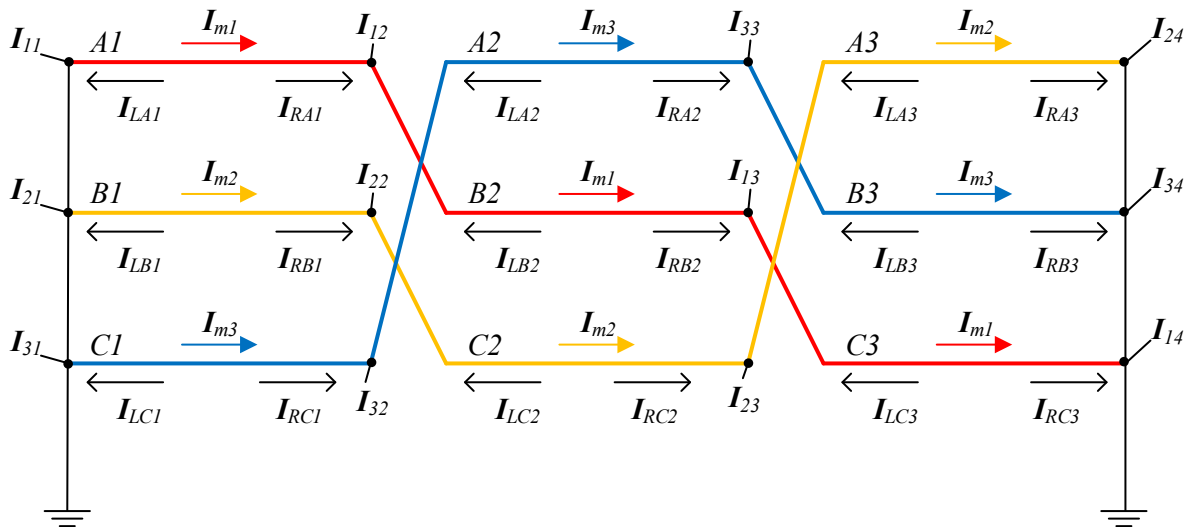

Fig. 6. The superimposed currents in the simplified cross-bonded sheath system

Where, referring to Fig.1, in sheath **loop 1**, I_{11} is the sheath current through the terminal TA1; I_{12} is the sheath current through the joint JA1; I_{13} is the sheath current through the joint JB2; I_{14} is the sheath current through the terminal TC2. In sheath **loop 2**, I_{21} is the sheath current through the terminal TB1; I_{22} is the sheath current through the joint JB1; I_{23} is the sheath current through the joint JC2; I_{24} is the sheath current through the terminal TA2. In sheath **loop 3**, I_{31} is the sheath current through the terminal TC1; I_{32} is the sheath current through the joint JC1; I_{33} is the sheath current through the joint JA2; I_{34} is the sheath current through the terminal TB2.

The sheath currents (I_{pq}, where p, q= 1, 2 or 3) at different points in loops 1, 2 and 3, assuming that positive current is from the power supply side to the load side, are presented in Equations (3) - (14).

$$I_{11} = +I_{LA1} + I_{LB2} + I_{LC3} - I_{m1} \tag{3}$$
$$I_{12} = -I_{RA1} + I_{LB2} + I_{LC3} - I_{m1} \tag{4}$$
$$I_{13} = -I_{RA1} - I_{RB2} + I_{LC3} - I_{m1} \tag{5}$$
$$I_{14} = -I_{RA1} - I_{RB2} - I_{RC3} - I_{m1} \tag{6}$$
$$I_{21} = +I_{LB1} + I_{LC2} + I_{LA3} - I_{m2} \tag{7}$$
$$I_{22} = -I_{RB1} + I_{LC2} + I_{LA3} - I_{m2} \tag{8}$$
$$I_{23} = -I_{RB1} - I_{RC2} + I_{LA3} - I_{m2} \tag{9}$$
$$I_{24} = -I_{RB1} - I_{RC2} - I_{RA3} - I_{m2} \tag{10}$$
$$I_{31} = +I_{LC1} + I_{LA2} + I_{LB3} - I_{m3} \tag{11}$$
$$I_{32} = -I_{RC1} + I_{LA2} + I_{LB3} - I_{m3} \tag{12}$$
$$I_{33} = -I_{RC1} - I_{RA2} + I_{LB3} - I_{m3} \tag{13}$$
$$I_{34} = -I_{RC1} - I_{RA2} - I_{RB3} - I_{m3} \tag{14}$$

2.5. Co-axial cables and detected currents

Fig. 7 is the practical connection of the cross-bonded cable system with 12 current sensors installed. Fig. 8 shows an expanded view of link box J1 and the currents detected by current sensor I_{2a}. Owing to the application of co-axial cables to connect joints and link boxes, a current sensor clamped on any co-axial cable will detect the vector sum of two different sheath currents, as presented in Fig. 8.
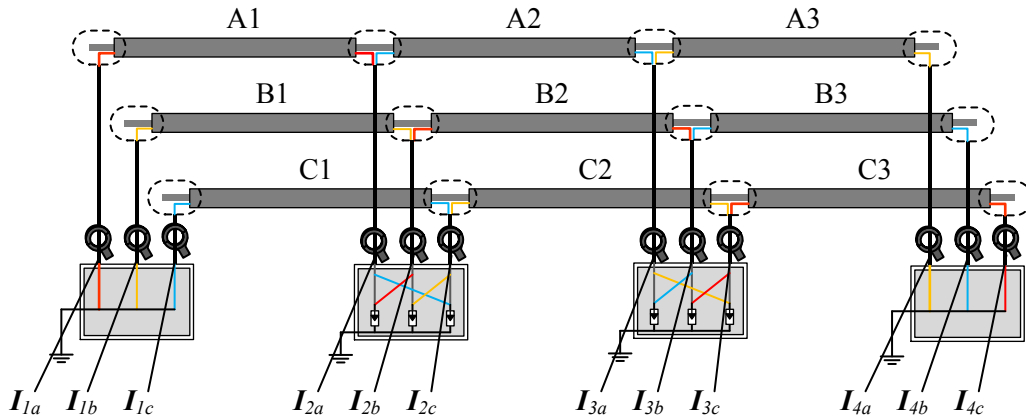

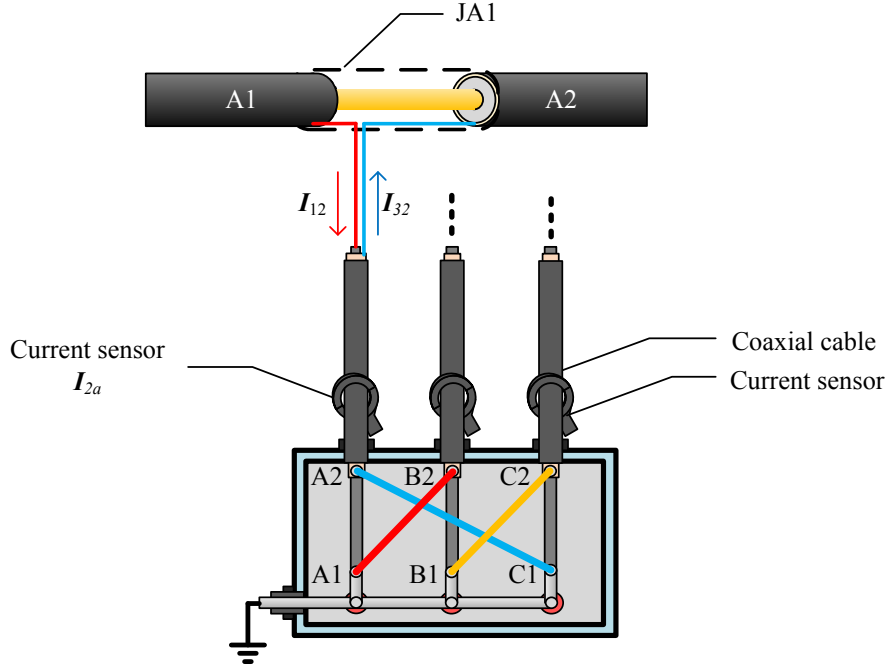Fig. 7. The installation of 12 current sensors in the major section

Fig. 8. The currents detected by the current sensor I_{2a} at the port of link box J1

Fig. 8 indicates that the core of the co-axial cable, on which the current sensor I_{2a} is clamped, connects to the metal sheath of A1, while the sheath of the co-axial cable connects to the metal sheath of A2. I_{2a} is the vector sum of I_{12} in sheath loop 1 (comprised of **A1**-B2-C3) and I_{32} in sheath loop 3 (comprised of C1-**A2**-B3).

As presented in Fig. 7 and Fig. 8, all the currents detected by the 12 current sensors can be expressed by the sheath currents, as presented in Equations (15) – (26).

$$I_{1a} = I_{11} \tag{15}$$
$$I_{1b} = I_{21} \tag{16}$$
$$I_{1c} = I_{31} \tag{17}$$
$$I_{2a} = I_{12} - I_{32} \tag{18}$$
$$I_{2b} = I_{22} - I_{12} \tag{19}$$
$$I_{2c} = I_{32} - I_{22} \tag{20}$$
$$I_{3a} = I_{33} - I_{23} \tag{21}$$
$$I_{3b} = I_{13} - I_{33} \tag{22}$$
$$I_{3c} = I_{23} - I_{13} \tag{23}$$
$$I_{4a} = I_{24} \tag{24}$$
$$I_{4b} = I_{34} \tag{25}$$
$$I_{4c} = I_{14} \tag{26}$$

Based on Equations (3) – (14) and (15) – (26), the currents detected by the 12 current sensors installed on the co-axial link cables can be expressed by a combination of circulating currents and leakage current components.

3. Leakage current separation method

3.1. Leakage current separation method principle

Section 2 outlined the complex relationship between of the sheath currents and the detected currents in a cross-bonded major section. In order to acquire the leakage current from each minor section, Leakage Current Separation Method (LCSM) is proposed. The schematic of the principle is presented in Fig. 9.
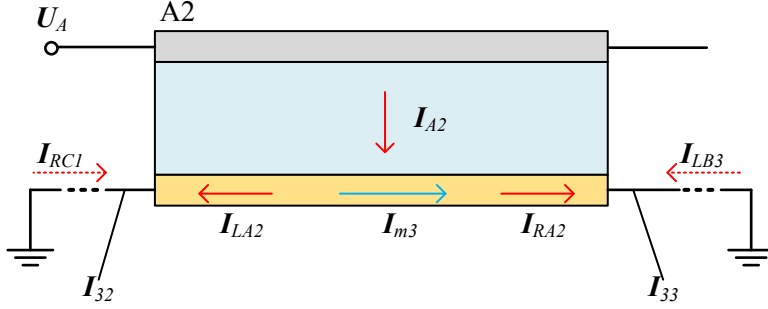

Fig. 9. Example: the schematic of the LCSM principle in minor section A2

Equation (27) indicates that the leakage current, I_{A2}, can be expressed by the sheath currents, I_{32} and I_{33}, as presented in Fig. 6, Equations (12) and (13).

$$
\begin{aligned}
I_{A2} &= I_{LA2} + I_{RA2} \\
&= (-I_{RC1} + I_{LA2} + I_{LB3} - I_{m3}) - (-I_{RC1} - I_{RA2} + I_{LB3} - I_{m3}) \\
&= I_{32} - I_{33}
\end{aligned}
\tag{27}
$$

This deduction is suitable for other 8 sections, as presented in Equations (28) – (35).

$$I_{A1} = I_{11} - I_{12} \tag{28}$$

$$I_{B2} = I_{12} - I_{13} \tag{29}$$

$$I_{C3} = I_{13} - I_{14} \tag{30}$$

$$I_{B1} = I_{21} - I_{22} \tag{31}$$

$$I_{C2} = I_{22} - I_{23} \tag{32}$$

$$I_{A3} = I_{23} - I_{24} \tag{33}$$

$$I_{C1} = I_{31} - I_{32} \tag{34}$$

$$I_{B2} = I_{33} - I_{34} \tag{35}$$

3.2. Improved LCSM results considering co-axial cables

In a cross-bonded cable system that uses six-import link boxes, it is possible to implement the leakage current separation for each minor section, as presented in Section 3.1. However, the utilization of the co-axial cables for connecting the joints and the link boxes makes it impossible to acquire the individual sheath currents. The detected currents should follow the principles and results in Section 2.5, as presented in Equations (15) – (26).

Although it is impossible to acquire the individual leakage current of each minor section, the current vector difference (e.g. I_{IBA}) can be derived from the detected currents (e.g. I_{1b}, I_{2b} and I_{1a}), as presented in Equation (36). Equation (36) is derived from Equations (28), (31), (16), (19) and (15).

$$I_{1BA} = I_{B1} - I_{A1}$$
$$= (I_{21} - I_{22}) - (I_{11} - I_{12})$$
$$= I_{21} - (I_{22} - I_{12}) - I_{11} \tag{36}$$
$$= I_{1b} - I_{2b} - I_{1a}$$

This is also applicable to the other 8 vector differences, as presented in Equations (37) – (44): these are derived from (27) – (35) and (15) – (26).

$$I_{1CB} = I_{C1} - I_{B1} = I_{1c} - I_{2c} - I_{1b} \tag{37}$$

$$I_{1AC} = I_{A1} - I_{C1} = I_{1a} - I_{2a} - I_{1c} \tag{38}$$

$$I_{2BA} = I_{B2} - I_{A2} = I_{2a} - I_{3b} \tag{39}$$

$$I_{2CB} = I_{C2} - I_{B2} = I_{2b} - I_{3c} \tag{40}$$

$$I_{2AC} = I_{A2} - I_{C2} = I_{2c} - I_{3a} \tag{41}$$

$$I_{3BA} = I_{B3} - I_{A3} = I_{3a} - I_{4b} + I_{4a} \tag{42}$$

$$I_{3CB} = I_{C3} - I_{B3} = I_{3b} - I_{4c} + I_{4b} \tag{43}$$

$$I_{3AC} = I_{A3} - I_{C3} = I_{3c} - I_{4a} + I_{4c} \tag{44}$$

Where, I_{nXY} is the vector difference between the leakage currents of the minor section Xn and Yn (X and Y stands for the different phases, e.g. A, B or C; n= 1, 2, 3).
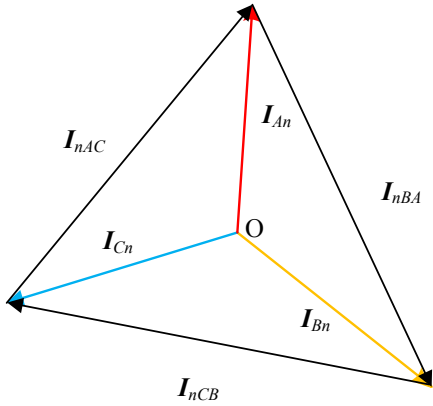

Fig.10. The vector diagram of the leakage currents and the leakage current vector differences

As shown in Fig. 10, I_{nBA} is the vector difference between leakage currents I_{Bn} and I_{An}, I_{nCB} is the vector difference between I_{Cn} and I_{Bn} and I_{nAC} is the vector difference between I_{An} and I_{Cn}.

Consequently, based on the detected currents from the 12 installed current sensors, the leakage current components can be separated from the sheath currents. The circulating currents are offset by the LCSM. Leakage current vector differences would be applied for further analysis.

3.3. Simulation of improved LCSM

In order to verify the improved LCSM (Equations (36) – (44)), simulations are carried out in MATLAB, based on the models presented in Fig. 11 and Fig. 12. The magnitudes of the phase voltages (U_A, U_B and U_C) are 63.5 kV (the phase-to-phase voltage is 110 kV). The phase difference among the operating voltages is $2\pi/3$. The earthing resistance near the power supply side is assumed to be 4 Ω. The earthing resistance near the load side is assumed to be 10 Ω. The manufacturer provides the factory parameter for

the XLPE insulated cables showing that the metal sheath impedance is 0.0426 Ω/km (20 °C), the initial insulation capacitance is 0.226 μF/km (20 °C), and the initial dielectric loss factor tan δ is 0.08%. The lengths of the three sections are, respectively, 425 m, 477 m and 536 m: these values replicat those in a practical cable network. The source resistances are 0.0001 Ω due to MATLAB requirement. And two set of simulations are presented. The induced voltages in the metal sheaths change with the RLC load parameters, as presented in Table 2 and 3.
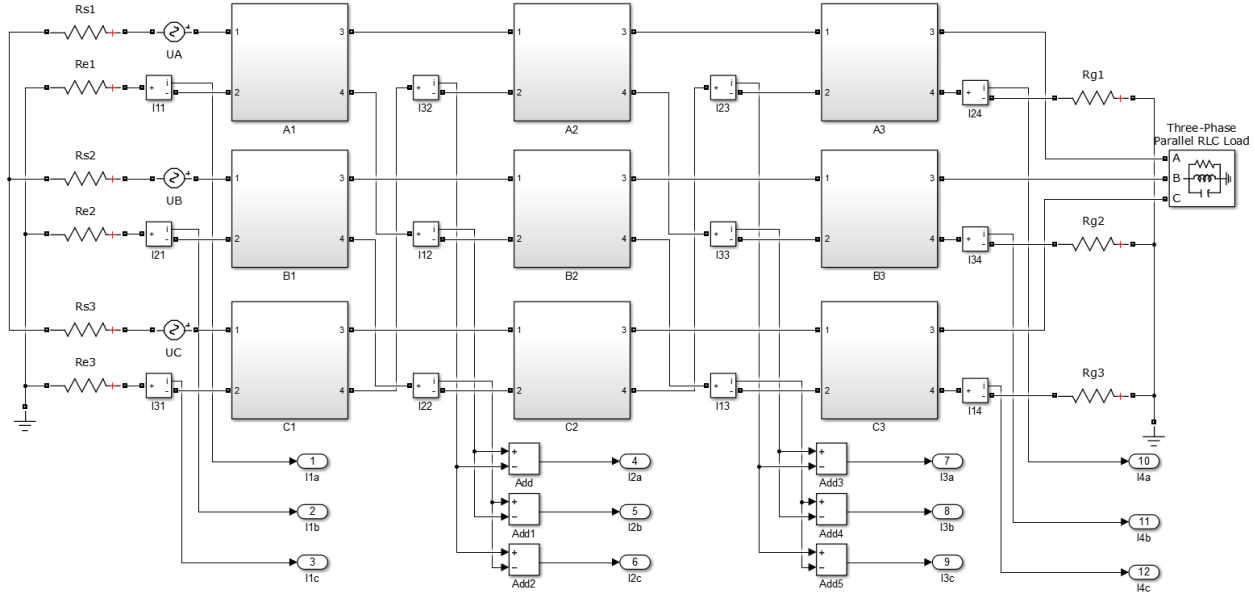

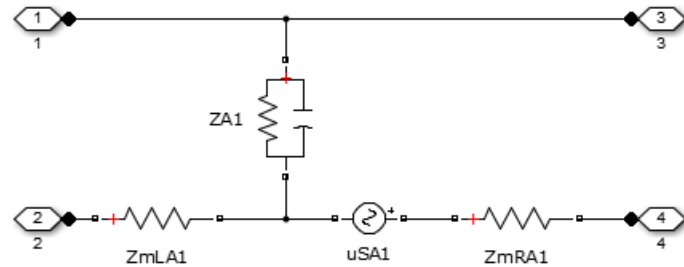Fig. 11. The simulation model in MATLAB Simulink derived from Fig. 7

Fig. 12. The subsystem of minor section A1 derived from Fig. 4

Table 1. Load information used in the two simulations (Y grounded)

Case	Load information
1	P=20 MW, Q=0 Mvar
2	P=20 MW, Q=8 Mvar

Table 2. The set of the induced voltages in sheaths in two simulations

Case	Parameter of the induced voltages in the sheath (V)								
	u_{SA1}	u_{SA2}	u_{SA3}	u_{SB1}	u_{SB2}	u_{SB3}	u_{SC1}	u_{SC2}	u_{SC3}
1	(-1.68 -5.74i)	(-4.64 +2.67i)	(+5.21 +5.45i)	(-4.13 +2.37i)	(+4.64 +4.85i)	(-2.12 -7.25i)	(+4.13 +4.32i)	(-1.89 -6.45i)	(-5.21 +3.00i)
2	(-1.81 -6.19i)	(-4.99 +2.87i)	(+5.61 +5.87i)	(-4.45 +2.55i)	(+5.00 +5.22i)	(-2.28 -7.81i)	(+4.45 +4.66i)	(-2.03 -6.95i)	(-5.61 +3.23i)

The induced voltages in sheaths calculation are based on the calculation in article [26].

10

Two set of the simulations based on Table 1 and Table 2 indicate that the change of load currents with the induced voltages have no effect on the leakage currents.

It should be noted that the temperature effect on the insulation of the load current has not been considered in the simulations. Assuming that the temperature effects are consistent across all cables, then when the temperature changes the insulation parameters, the LCSM results can also reflect the variations.

Fig. 14 presents the waveforms of leakage currents of the minor sections A1 and B1. I_{A1} and I_{B1} are the currents acquired from the insulation impedance branch directly (e.g. the ZA1 branch shown in Fig. 12). I_{1b}, I_{2b} and I_{1a} are the currents acquired by the installed current sensors (shown in Fig. 11).
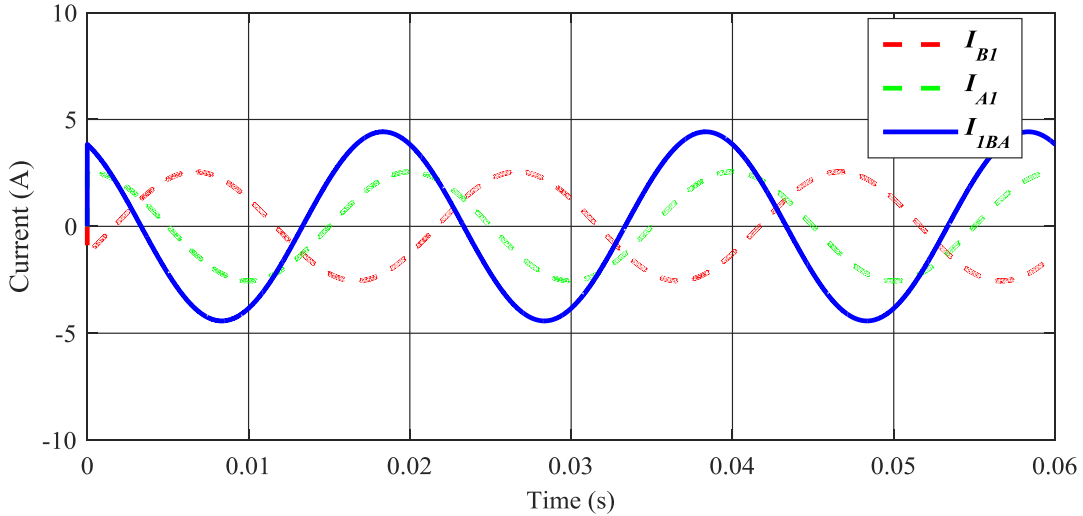
(a) The theoretical result of leakage current vector difference between minor section A1 and B1
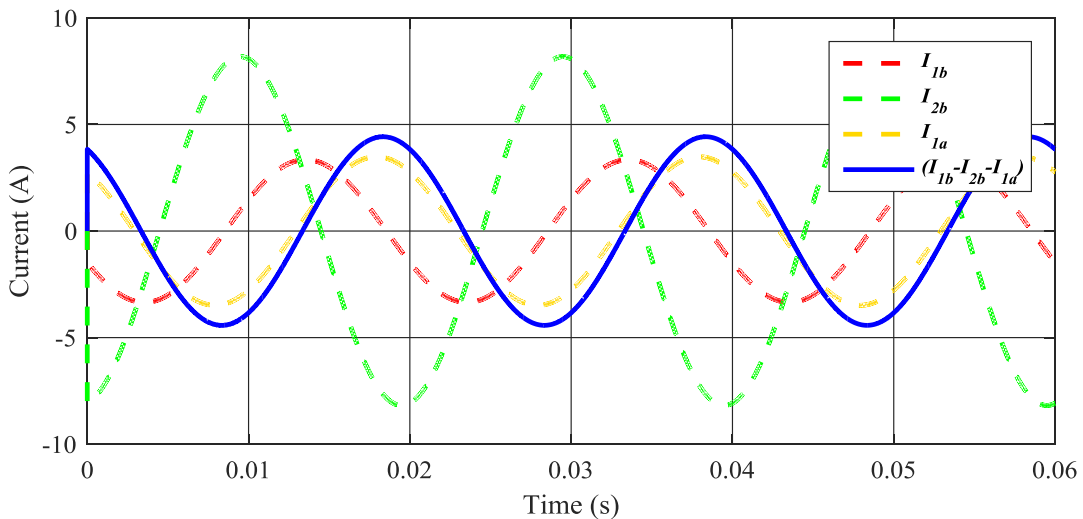
(b) The detected currents and the improved LCSM result for I_{1BA}

Fig. 14. Example: the comparison results of I_{1BA}

The comparison of the data presented in Fig. 14 (a) and (b) indicates that the magnitude and phase of $(I_{1b} - I_{2b} - I_{1a})$ and I_{1BA} are nearly the same: the degree of difference is listed in Table 3. The results presented in Table 3 demonstrate that the method is applicable for all minor sections in the cross-bonded major section.

In Table 3, the expected results denote the results from the definition, i.e. the expected result of I_{1BA} is the vector difference between I_{B1} and I_{A1} ($I_{1BA} = I_{B1}-I_{A1}$). Improved LCSM results denote the results from leakage current separation ($I_{1BA} = I_{1b}-I_{2b}-I_{1a}$).

Table 3. The comparison between the improved LCSM results and the expected results

Deduced current	Improved LCSM RMS results (A)	Expected RMS results (A)	Error (%)
I_{1BA}	$|I_{1b}-I_{2b}-I_{1a}|=3.1286397$	$|I_{B1}-I_{A1}|=3.1286327$	2.23×10^{-4}
I_{1CB}	$|I_{1c}-I_{2c}-I_{1b}|=3.1287618$	$|I_{C1}-I_{B1}|=3.1287528$	2.87×10^{-4}
I_{1AC}	$|I_{1a}-I_{2a}-I_{1c}|=3.1285671$	$|I_{A1}-I_{C1}|=3.1285376$	9.42×10^{-4}
I_{2BA}	$|I_{2a}-I_{3b}|=3.5110974$	$|I_{B2}-I_{A2}|=3.5110830$	4.10×10^{-4}
I_{2CB}	$|I_{2b}-I_{3c}|=3.5113462$	$|I_{C2}-I_{B2}|=3.5113418$	1.24×10^{-4}
I_{2AC}	$|I_{2c}-I_{3a}|=3.5112081$	$|I_{A2}-I_{C2}|=3.5111955$	3.58×10^{-4}
I_{3BA}	$|I_{3a}-I_{4b}+I_{4a}|=3.9457919$	$|I_{B3}-I_{A3}|=3.9457772$	3.71×10^{-4},
I_{3CB}	$|I_{3b}-I_{4c}+I_{4b}|=3.9460412$	$|I_{C3}-I_{B3}|=3.9460248$	4.15×10^{-4}
I_{3AC}	$|I_{3c}-I_{4a}+I_{4c}|=3.9458874$	$|I_{A3}-I_{C3}|=3.9458766$	2.72×10^{-4}

As presented in Table 3, the difference between the improved LCSM results (Equations (36) – (44)) and the expected results is less than 1×10^{-3} %. As this is the simulation in normal condition, the expected deduced current maganitudes in the same section (e.g. I_{1BA}, I_{1CB} and I_{1AC}) are the same, as the length and the insulation impedance are assumed to be the same. The maximum RMS difference between deduced currents (e.g. I_{1BA}, I_{1CB} and I_{1AC}) in the same section is less than 0.01 %. This work verifies the feasibility of separating the leakage current components from the detected currents by the LCSM. It should be noted that the proposed separation method is not confined to the cross-bonded system analysed above.

4. Relative DL angle based on the leakage current vector differences

In operational power cable transmission systems, as mentioned in Section 1, it is hard to get the operating voltage from the power cable directly due to the safety issues. If the voltage signals are detected from substations, there will be unmeasurable difference between the detected voltage signal and the voltage at the cable terminals or the joints.

A method based on a comparison of leakage current vector difference is proposed to determine the relative change of DL, instead of the absolute value. This solves the challenge of situations where measuring the reference voltage vector is not possible.

The DL factor can be expressed by the equivalent insulation resistance and insulation capacitance, as shown in Equation (45).

$$\tan\delta = \frac{1}{\omega RC} \tag{45}$$

Where, R is the equivalent insulation resistance; C is the equivalent insulation capacitance and ω is the angular frequency.

Any change of the insulation impedance (R and C) affects the DL factor, as presented in Equation (45). In Fig. 15, the operating voltage vector is assumed to be unchanged as a reference line. The leakage current vector would change due to the change of dielectric loss angle, from δ to δ'.
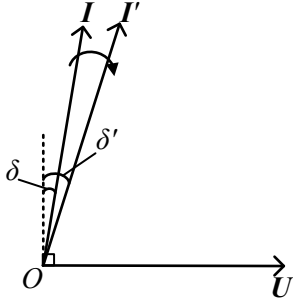
Fig. 15. The vector diagram of the DL angle during the insulation deterioration

It was noted in [2] and [18] that, as a result of moisture deterioration in XLPE insulation, DL factor shows an increasing trend due to the decrease of the insulation resistance. In other insulation deterioration, such as thermal deterioration [19], mechanical deterioration [25], oxidation deterioration [24], radiation deterioration and electrical deterioration [23], the indications are that insulation capacitance does not change much during the deterioration. Increase in the DL angle results from decrease in the insulation resistance, such as in the case of water tree aging due to moisture deterioration.

The change of the leakage current vector can be applied to the assessment of the insulation condition. Larger DL angle and larger leakage current magnitude indicates poorer insulation condition. When this judgement is applied to the three-phase condition, the reference voltage can be avoided. Fig. 16 indicates that the changes in the DL angles results in changes in the leakage current vectors (I_A, I_B and I_C) and also to changes in the leakage current vector differences (I_{BA}, I_{CB} and I_{AC}).
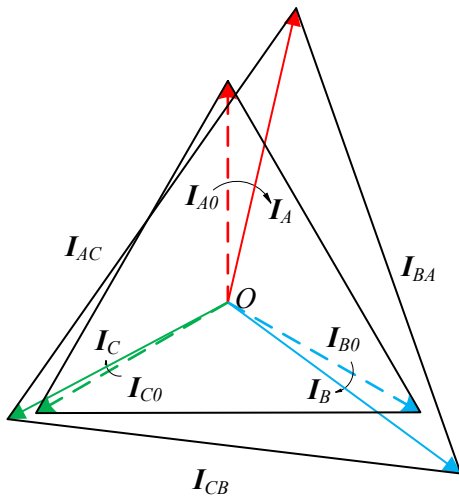

Fig. 16. Relative changes of DL angles leading to the changes in the leakage current vector differences

Table 4 presents a set of rules to assess the insulation condition, based on the leakage current vector differences. The rules were developed from the simulations in MATLAB, based on the assumptions shown below.

● The insulation materials of three phases are the same type.
● The variation of DL angle is due to the change in insulation resistance.

Table 4 transfers the vector length relationship to a DL angle relationship. The relative insulation condition is based on the order of DL angles among three phases in the first column of Table 4. These

criteria could provide a rapid qualitative description of the relative insulation condition.

Table 4. Simulation results and the criteria for the relative insulation condition among three phases

Order of DL angles among three phases	Vector length order	Relative insulation condition
$\delta_B < \delta_C < \delta_A$ $\delta_C < \delta_B < \delta_A$	$I_{AC} > I_{CB} > I_{BA}$	Phase A is the worst
$\delta_A < \delta_C < \delta_B$ $\delta_C < \delta_A < \delta_B$	$I_{BA} > I_{AC} > I_{CB}$	Phase B is the worst
$\delta_B < \delta_A < \delta_C$ $\delta_A < \delta_B < \delta_C$	$I_{CB} > I_{BA} > I_{AC}$	Phase C is the worst
$\delta_A < \delta_B < \delta_C$ $\delta_A < \delta_C < \delta_B$	$I_{BA} > I_{CB} > I_{AC}$	Phase A is the healthiest
$\delta_B < \delta_C < \delta_A$ $\delta_B < \delta_A < \delta_C$	$I_{CB} > I_{AC} > I_{BA}$	Phase B is the healthiest
$\delta_C < \delta_B < \delta_A$ $\delta_C < \delta_A < \delta_B$	$I_{AC} > I_{BA} > I_{CB}$	Phase C is the healthiest

In Table 4, when the RMS values of the leakage current vector differences accord with the relationship, $I_{AC} > I_{CB} > I_{BA}$, this is an indication that the dielectric loss angle of A is larger than that of B and C, although the relationship between the DL angle of B and of C is uncertain ($\delta_B < \delta_C < \delta_A$ or $\delta_C < \delta_B < \delta_A$). Thus, the indication is that "the relative deterioration in phase A is the worst".

The process outlined in Sections 3 and 4 could be implemented as an on-line monitoring system for insulation condition, as present in Fig. 17. To verify the feasibility of application in practical systems, this method has been applied in a 110-kV cross-bonded cable in a tunnel, as discussed in Section 5.
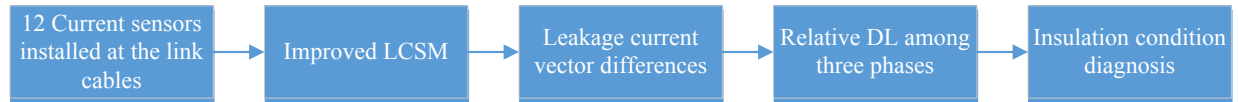

Fig. 17. The flowchart of on-line monitoring dielectric loss in cross-bonded HV cable system

5. Case study

The on-line monitoring system based on the proposed plan was applied to a 110-kV XLPE power cable tunnel in Wuhan, China. The lengths of the three sections in the major section were 425 m, 477 m and 536 m, as discussed in Section 3.3. Due to the expenditure issues, there were only 6 current sensors installed at the co-axial cables connected to the link boxes, J1 and J2. Data was collected from December 2014 to July 2016. The sampling rate was 100 MS/s. The sampling length was 2 s, and the sampling interval was 6 min, i.e. there were 240 sample points every day.

5.1. Detected currents

Fig. 18 shows the raw data from the current sensors I_{2a}, I_{2b}, I_{2c}, I_{3a}, I_{3b} and I_{3c}, corresponding to those in Fig. 7. Fig. 18(a) is the data collected on 15th December, 2014; Fig. 18(b) is the data collected on 26th March, 2015; Fig. 18(c) is the data collected on 23rd May, 2015; Fig. 18(d) is the data collected on 13th September, 2015; and Fig. 18(e) is the data collected on 7th June, 2016.
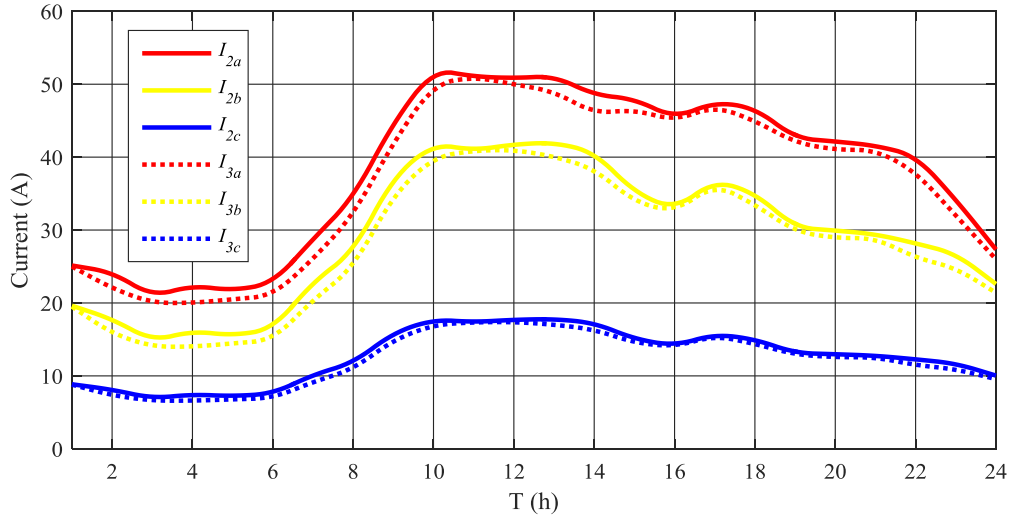
(a) The detected current RMS values on 15th December, 2014
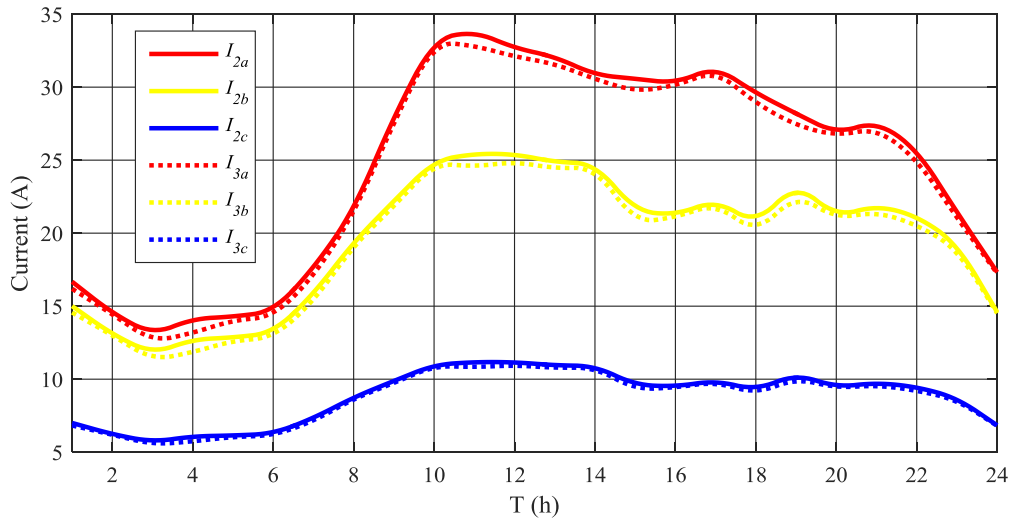
(b) The detected current RMS values on 26th March, 2015
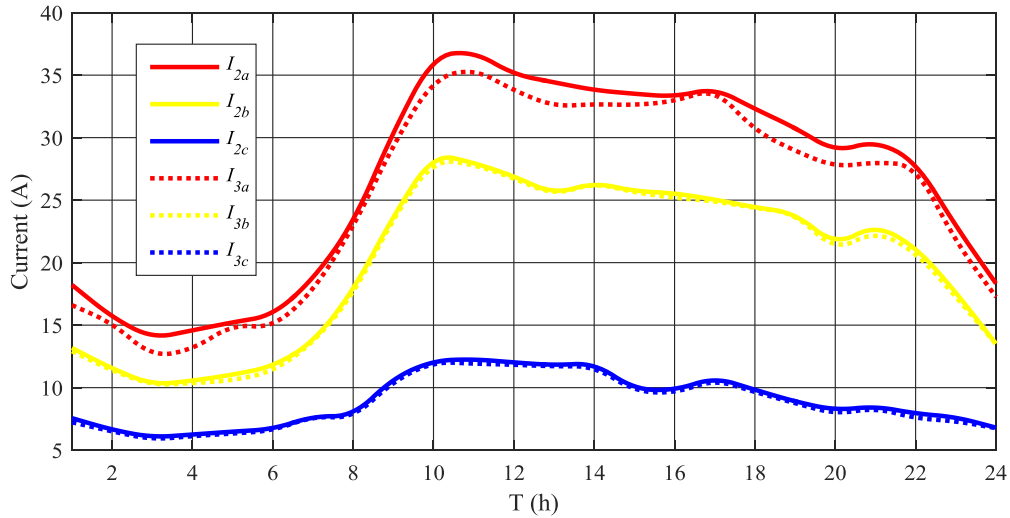
(c) The detected current RMS values on 23rd May, 2015

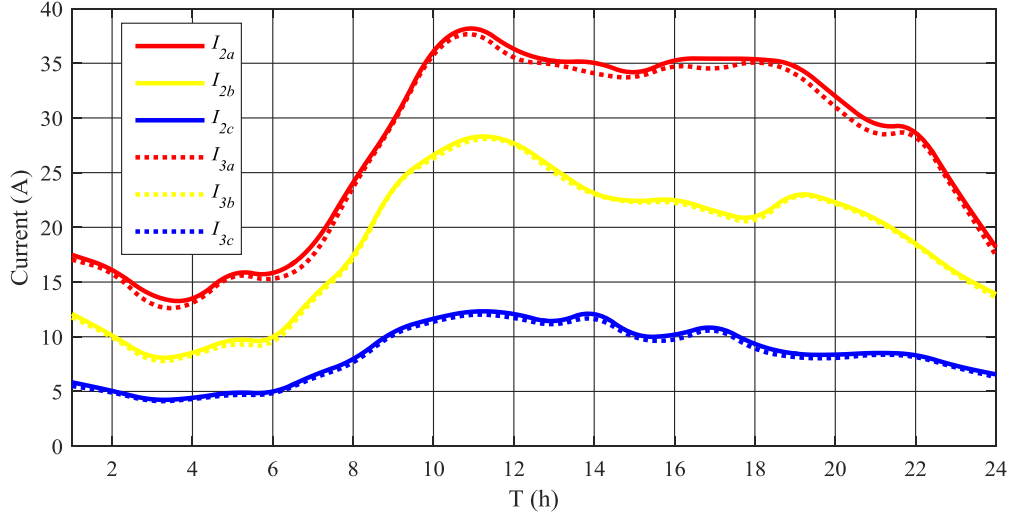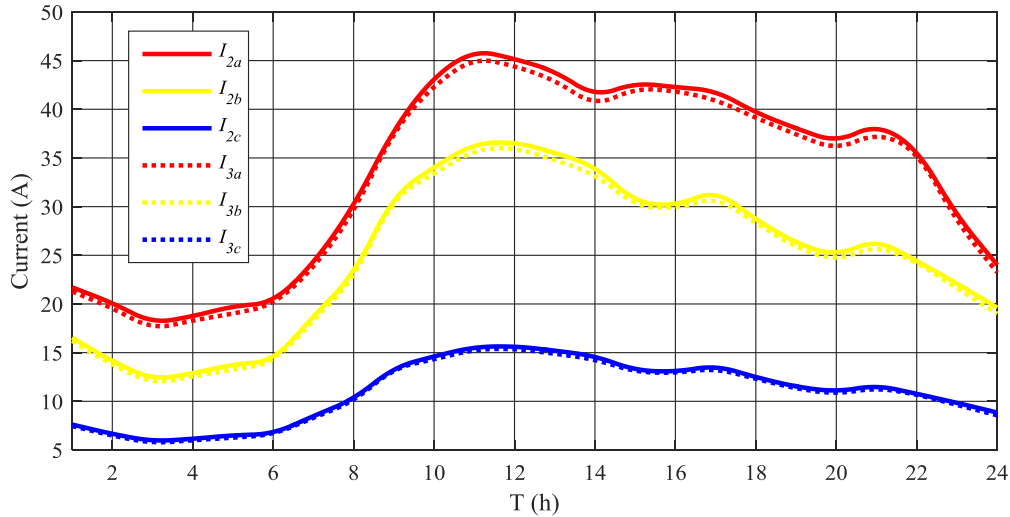(d) The detected current RMS values on 13th September, 2015

(e) The detected current RMS values on 7th June, 2016

Fig. 18. The RMS values of currents detected by the current sensors

In Fig. 18, each of the figures presents the RMS values of 6 detected currents detected from the co-axial cables connected to J1 and J2. It should be noted that the detected currents are all the waveforms rather than the RMS values, which are calculated for reporting here. Fig. 18 displays several characteristics which are presented below.

Firstly, the layout of the studied major section was not symmetrical. The length of each sub-section in this major section was different: sub-sections 1, 2 and 3 had the lengths of 425m, 477m and 536m respectively. The three-phase single-core cables were laid in a flat configuration and the load currents of the three phases were unbalanced. These factors lead to an imbalance in the induced voltage in the sheath loops, causing the relatively high circulating currents.

Secondly, due to the unequal circulating currents in different sheath loops, there is a big difference among the different detected currents, e.g. the data on 7th June 2016 indicated that $I_{2a} > I_{2b} > I_{2c}$.

Thirdly, because of the daily fluctuation of load currents, there were big variances in detected currents over the course of a day. As discussed in Section 2.3, the circulating currents, which are the main

16

components of the sheath currents, are influenced by the load currents.

Fourthly, due to the seasonal fluctuation of load currents (winter in December, spring in March and May, summer in June and autumn in September for this location), the ranges of the detected currents vary considerably. The maximum measured current in December was over 50 A, while the maximum measured current in April and May was just 30 A. The load currents in spring and autumn in this location were similar.

Finally, the detected currents I_{2x} were a little bit higher than I_{3x} (x stands for a, b and c) due to the ground resistance near the source side being smaller than that near load side. Consequently, leakage currents components were flowing more to the source side.

5.2. Improved LCSM results

Based on the on-line measured data, the leakage current vector differences were deduced by the improved LCSM. The results would be influenced by the fluctuation of the operation voltage, Ux, as presented in Fig. 4. Based on regulation GB 12326-2008, the National Standard in China which is in accordance with IEC standard, the system voltage fluctuation is prescribed to be less than 2% at the voltage level 110 kV. So, to describe the relative aging over the course of a day, the average value was used to offset the influence of the voltage fluctuation, as presented in Fig. 19.

Fig. 19(a) is the calculated data for 15th December, 2014; Fig. 19(b) is the calculated data for 26th March, 2015; Fig. 19(c) is the calculated data for 23rd May, 2015; Fig. 19(d) is the calculated data for 13th September, 2015; Fig. 19(e) is the calculated data for 7th June, 2016.
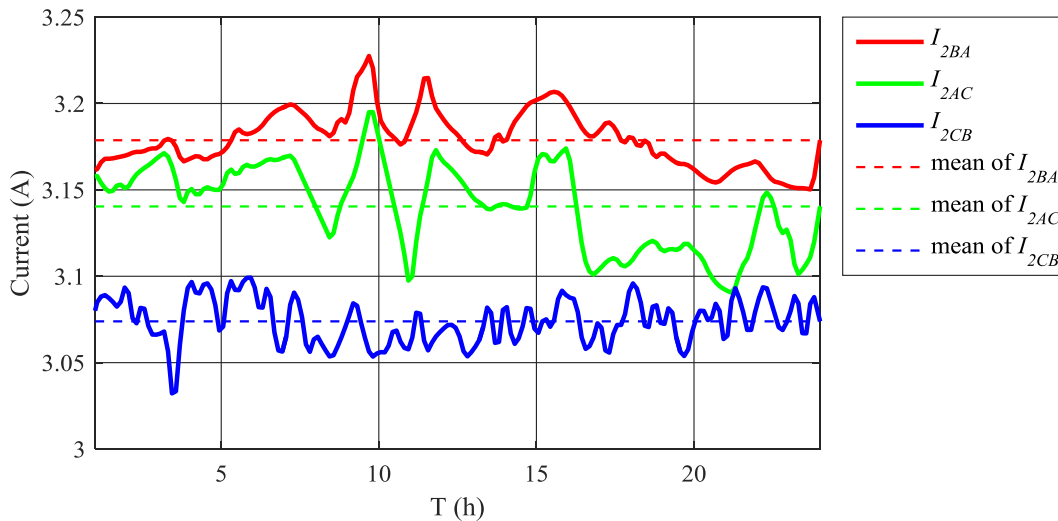
(a) The RMS values of leakage current vector differences on 15th December, 2014
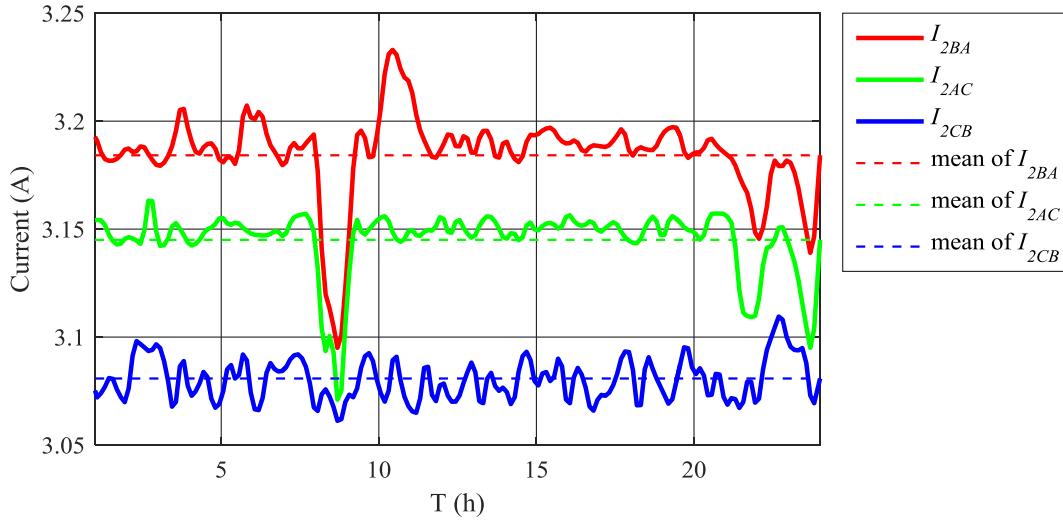
(b) The RMS values of leakage current vector differences on 26th March, 2015
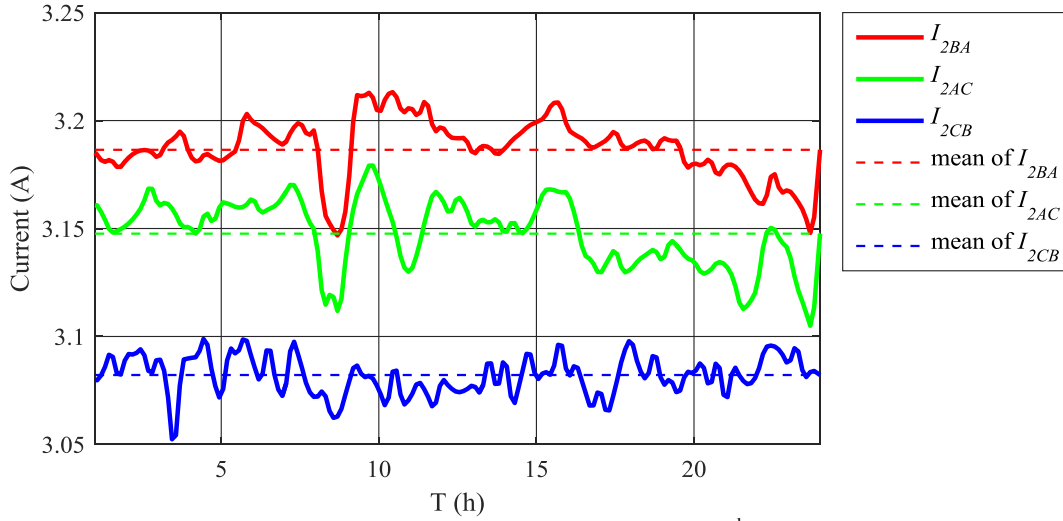
(c) The RMS values of leakage current vector differences on 23rd May, 2015

(d) The RMS values of leakage current vector differences on 13th September, 2015

(e) The RMS values of leakage current vector differences on 7th June, 2016

Fig. 19. Comparison of the RMS values of leakage current vector differences

It should first be noted that, as the fluctuation of the operational voltage might lead to a variation in the results, the average RMS values from the 24-hours collection were used for comparison purpose.

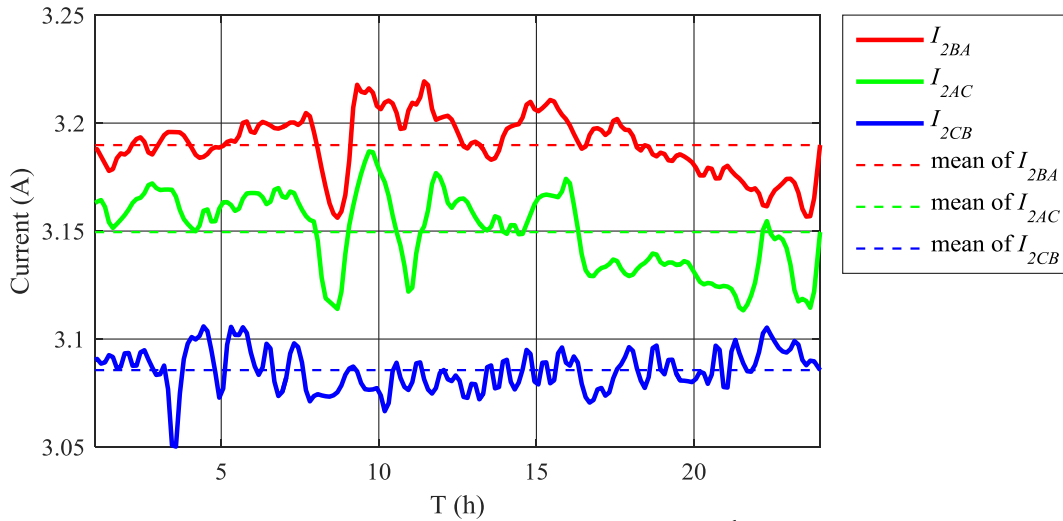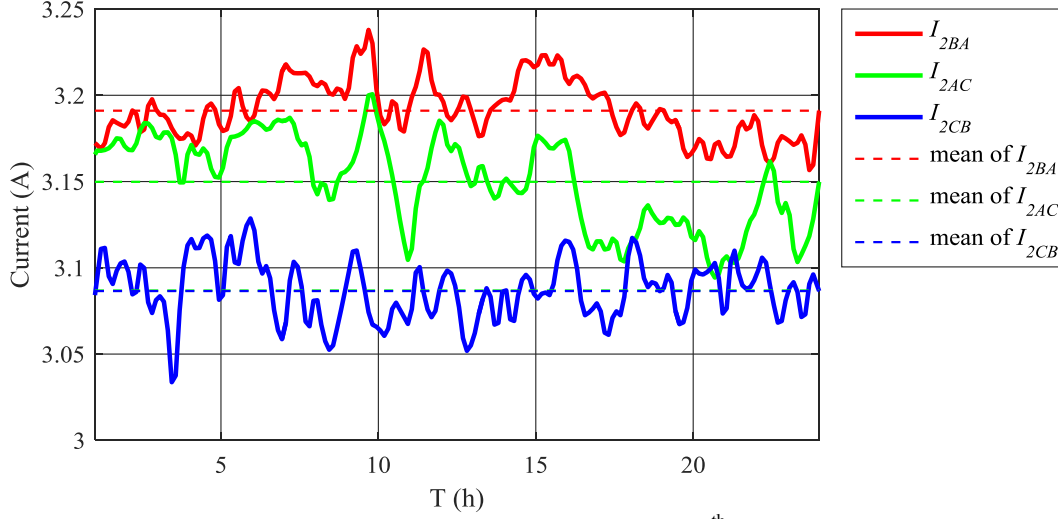Secondly, in the majority of cases, the relationship among I_{2BA}, I_{2CB} and I_{2AC} satisfied the condition that $I_{2BA} > I_{2AC} > I_{2CB}$. However, some data did not meet the situation, e. g. at 08:36 on 26th March, 2015 and at 20:54 on 7th June, 2016, the RMS value of I_{2BA} is less than that of I_{2AC}.

Thirdly, in most of cases, the fluctuation of I_{2BA}, I_{2CB} and I_{2AC} did not exceed ± 2 % of the average RMS value of each leakage current vector differences. However, for several points, e. g. at 08:36 on 26th March, 2015, the fluctuation of the RMS value of I_{2BA} and I_{2AC} was around 3%. This may be the short-period voltage fluctuation.

5.3. Analysis and summary

As indicated in Fig. 19, during the periods analysed, the relationship shown in (46) holds for the majority of data the time on all dates.

$$I_{2BA} > I_{2AC} > I_{2CB} \tag{46}$$

As can be seen, it is better to be apply the mean value of each deduced current to describe the relative insulation condition among three phases, to offset the influence of periodic fluctuation. The average RMS values for the cross-bonded cable system investigated are presented in Table 5.

Table 5. Comparison of average values among phases during monitoring period

Data collected	December, 2014	March, 2015	May, 2015	September, 2015	June, 2016
I_{2BA} (A)	3.1787	3.1841	3.1864	3.1898	3.1910
I_{2CB} (A)	3.0739	3.0808	3.0821	3.0856	3.0865
I_{2AC} (A)	3.1404	3.1450	3.1476	3.1495	3.1498

As presented in Fig. 20, during the monitoring period from December, 2014 to June, 2016, the relationships among I_{2BA}, I_{2CB} and I_{2AC} satisfied the condition that $I_{2BA} > I_{2AC} > I_{2CB}$. Based on the criteria in Table 4, the long-term results indicated that the minor section B2 deteriorated faster than other two minor sections in section 2,
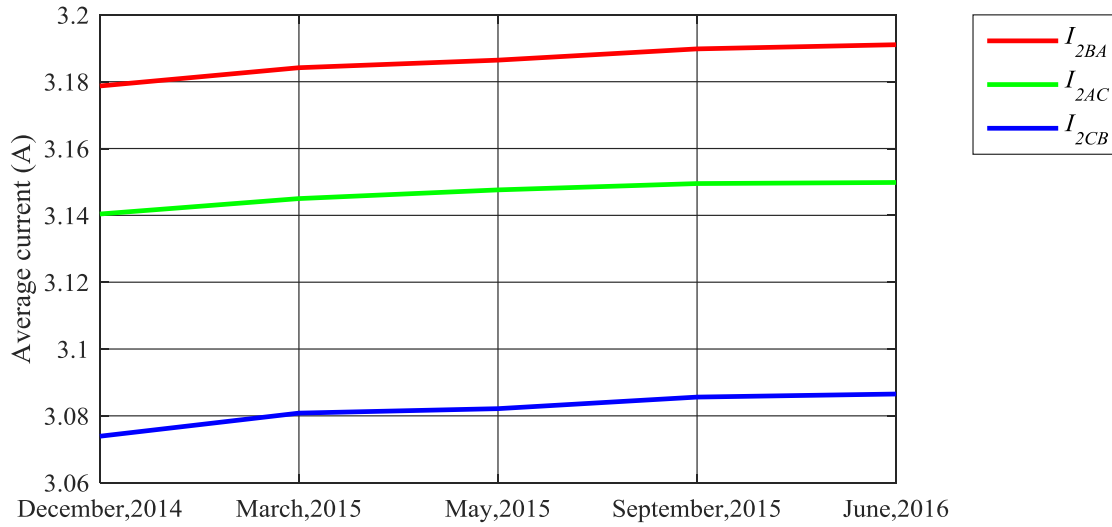
Fig. 20. The trending of the leakage current vector differences

Moreover, over the period of the investigation, the average values of deduced currents were increasing. I_{2BA} in June, 2016 was 0.39 % higher than in December, 2014. I_{2AC} in June, 2016 was 0.30 % higher than in December, 2014. I_{2CB} in June, 2016 was 0.41 % higher than in December, 2014. This indicated that all three minor sections had a certain degree of deterioration during the measurement. As previously mentioned, the leakage current from B2 grew faster than that from A2 and C2.

Over the same 18 month period another form of condition assessment, i.e. Partial Discharge (PD) monitoring, was carried out in this major section and there was no indication of significant deterioration. However, as insulation degradation processes occur over long periods, a long-term observation is needed to see whether deterioration is occurring. The long term case study of on-line monitoring of this major cable section indicates that it is feasible to use the relative DL to determine the relative insulation condition among three phases for a cross-bonded cable system.

6. Conclusion

This work proposes a novel method of on-line monitoring of relative insulation condition in a major section of a cross-bonded network by the installation of 12 current sensors on the co-axial cables connecting link boxes and joints or terminals.

The novel Leakage Current Separation Method (LCSM) achieves the separation of the leakage currents in the cross-bonded system with the application of current sensors to the co-axial cables connecting the link boxes and joints.

The LCSM simulation results indicate that an RLC load had no effect on the leakage current separation results. Moreover, variation in the lengths of the cables in different sections had no effect on the accuracy of the method.

The increase in DL angles will lead to the change in leakage current vectors. In addition, the variation of the leakage current vectors will lead to the change of the leakage current vector difference. Relative DL among three phases method to determine the insulation condition is based on the results of leakage current vector difference among three phases.

The success of the proposed methods in the case study indicates the feasibility of carrying out long term

on-line monitoring. Analysis indicates that there is no significant deterioration of the cables under study. However, minor section B2 should have more attention paid to it. As the cables are at the start of their operational life, continued monitoring will be carried out to ensure cables remain suitable for use.

The limitation of the work is that diagnosis based on DL has disadvantages in the detection of partial deterioration. Some insulation faults that lead to an obvious variation in leakage current could also be detected. As such, different on-line techniques should work complementarily to assess insulation condition.

References

[1] Bojie Sheng, Wenjun Zhou, Jianhui Yu, Shaoxin Meng, Chengke Zhou and D. Hepburn, "On-line PD detection and localization in cross-bonded HV cable systems", *IEEE Transactions on Dielectrics and Electrical Insulation*, vol. 21, no. 5, pp. 2217-2224, 2014. X. Dong, Y. Yuan, Z. Gao, C. Zhou, B. Sheng, H. Zhao, Analysis of cable failure modes and cable joint failure detection via sheath circulating current, Electrical Insulation Conference (EIC), 2014, pp. 294-298.

[2] R. Jiang, "Aging mechanisms and monitoring of XLPE insulated power cable" in *XLPE power cable lines*, 2nd ed. Beijing, China, China Electric Power Press, 2009.

[3] H. Zhang, "110-220kV XLPE cable insulation on-line monitoring technique", ph.D dissertation, Wuhan University, SEE, Wuhan, China, 2009.

[4] Bojie Sheng, Chengke Zhou, D. Hepburn, Xiang Dong, G. Peers, Wenjun Zhou and Zeyang Tang, "Partial discharge pulse propagation in power cable and partial discharge monitoring system", *IEEE Transactions on Dielectrics and Electrical Insulation*, vol. 21, no. 3, pp. 948-956, 2014. IEEE Draft guide for bonding shields and sheaths of single-conductor power cables rated 5 kV through 500kV, IEEE P575/D11, 2013, pp.1-80.

[5] B. Pang, B. Zhu, X. Wei, S. Wang, and R. Li, "On-line monitoring method for long distance power cable insulation," *IEEE Trans. Dielectr. Electr. Insul.*, vol. 23, no. 1, pp. 70–76, Feb. 2016.

[6] M. Marzinotto and G. Mazzanti, "The Feasibility of Cable Sheath Fault Detection by Monitoring Sheath-to-Ground Currents at the Ends of Cross-Bonding Sections," *IEEE Trans. Ind. Appl.*, vol. 51, no. 6, pp. 5376–5384, Nov. 2015.

[7] Chengke Zhou, Wenjun Zhou, D. M. Hepburn, Bojie Sheng, Xiang Dong, and B. Alkali, "PD detection and localisation in cross-bonded HV cable systems," in *22nd International Conference and Exhibition on Electricity Distribution (CIRED 2013)*, 2013, pp. 0129–0129.

[8] P. Fa-dong, Y. Li, X. Li, C. Yong-hong, C. Xu-sheng, C. Xiao-lin, and M. Yong-peng, "The Design of Distributed On-line Monitoring System for Metal Sheath's Circulating Current of Cross-linked Power Cables," in *2008 International Conference on High Voltage Engineering and Application*, 2008, pp. 562–565.

[9] *IEEE Draft Standard Environmental and Testing Requirements for Communications Networking Devices Installed in Transmission and Distribution Facilities*, IEEE P1613.1/D47, 2013, pp. 1-20.

[10] B. Sheng, C. Zhou, D. M. Hepburn, X. Dong, W. Zhou, and J. Yu, "Investigation of partial discharge propagation in cross-bonded HV cable systems," in *2014 IEEE Electrical Insulation Conference (EIC)*, 2014, pp. 19–23.

[11] Y. Yang, D. M. Hepburn, W. Jiang, B. Yang, C. Zhou, and W. Zhou, "On-line monitoring and relative trending of dielectric loss in cross-linked HV cable systems," in *9th Jicable*, 2015.

[12] Y. Yang, D. M. Hepburn, C. Zhou, W. Jiang, B. Yang, and W. Zhou, "On-line monitoring and trending of dielectric loss in a cross-bonded HV cable system," in *2015 IEEE 11th International Conference on the Properties and Applications of Dielectric Materials (ICPADM)*, 2015, pp. 301–304.

[13] *IEC standard voltages*, IEC 60038, 2009.

[14] Z. Li, X. Chu, X. Zeng, and N. Chen, "A New On-line Measurement System of Dielectric Loss Angle for High Voltage Capacitive Apparatus," in *2007 IEEE Industry Applications Annual Meeting*, 2007, pp. 1512–1516.

[15] N. Wang, F. C. Lu, and H. M. Li, "Analytical processing of on-line monitored dissipation factor based on morphological filter," *IEEE Trans. Dielectr. Electr. Insul.*, vol. 11, no. 5, pp. 840–846, Oct. 2004.

[16] *Electric cables- calculation of the current rating-Part 1-1: Current rating equations (100% load factor) and calculation of losses- general*, IEC 60287-1-1, second edition, 2006-12.

[17] X. Huang, X. Hu, "Comprehensive relative measurement method in dielectric loss-line Detection", *High voltage electrical appliances*, June, 2001.

[18] H. Wang, S. Cheng, X. Wen, "AC Insulation Characteristic of XLPE in the Course of Aging", *High Voltage Engineering*. Mar, 2005.

[19] H.-X. Wang, Y.-L. Wang, and A.-Z. Han, "Insulation Parameters Characteristics of XLPE Cable in the course of Its Aging within CuSO4 Electrolyte," in *2008 International Conference on High Voltage Engineering and Application*, 2008, pp. 331–334.

[20] J. Fothergill, S. Dodd, L. Dissado, T. Liu, and U. Nilsson, "The measurement of very low conductivity and dielectric loss in XLPE cables: a possible method to detect degradation due to thermal aging," *IEEE Trans. Dielectr. Electr. Insul.*, vol. 18, no. 5, pp. 1544–1553, Oct. 2011.

[21] M. German-sobek, R. Cimbala, and J. Király, "Change of Dielectric Parameters of XLPE Cable due to Thermal Aging," *Electroteh. Electron. Autom.*, vol. 62, no. 3, pp. 47–53, 2014.

[22] H. Djidjelli, M. Kaci, A. Boukerrou, D. Benachour, and J. J. Martinez-Vega, "Hydrothermic aging of plasticized poly(vinyl chloride): Its effect on the dielectric, thermal, and mechanical properties," *J. Appl. Polym. Sci.*, vol. 89, no. 13, pp. 3447–3457, Sep. 2003.

[23] Z. Ma, X. Huang, P. Jiang, and G. Wang, "Effect of silane-grafting on water tree resistance of XLPE cable insulation," *J. Appl. Polym. Sci.*, vol. 115, no. 6, pp. 3168–3176, Mar. 2010.

[24] C. Kim, Z. Jin, P. Jiang, Z. Zhu, and G. Wang, "Investigation of dielectric behavior of thermally aged XLPE cable in the high-frequency range," *Polym. Test.*, vol. 25, no. 4, pp. 553–561, 2006.

[25] V. Plaček, T. Kohout, J. Kábrt, and J. Jiran, "The influence of mechanical stress on cable service life-time," *Polym. Test.*, vol. 30, no. 7, pp. 709–715, 2011.

[26] X. Dong, Y. Yang, C. Zhou, and D. M. Hepburn, "On-line Monitoring and Diagnosis of HV Cable Faults by Sheath System Currents," *IEEE Trans. Power Deliv.*, vol. 8977, no. c, pp. 1–1, 2017.

Yang Yang received the B.Sc. degree from the School of Automation, Wuhan University of Technology, China, in 2013, and the M.Sc. degree in School of Electrical Engineering, Wuhan University, China, in 2016. Now he is a Ph. D. student in Glasgow Caledonian University, who is mainly research on the development of the measurement of insulation condition, including dielectric loss, leakage current and insulation resistance.

Chengke Zhou received the B.Sc. and M.Sc. degrees in Hydropower Automation from Huazhong University of Science and Technology, Wuhan, China, in 1983 and 1986, respectively, and the Ph.D. degree in Electrical Science from The University of Manchester, Manchester, U.K., in 1994.

He joined the School of Engineering and Computing, Glasgow Caledonian University (GCU), in Glasgow, U.K. in 1994 and was a Post-doctoral Research Fellow, Lecturer, and Senior Lecturer until 2006 when he joined Heriot-Watt University as a Reader in Edinburgh, Scotland, UK. In 2007, he returned to GCU as a Professor. He has more than 20 years of research experience in power systems and partial-discharge-based high-voltage plant condition monitoring and has acted as a Consultant to EDF Energy, Scottish Power plc, and British Energy. So far, he has published more than 100 papers.

Dr. Zhou is a Fellow of IET and a Chartered Engineer and Senior Member of IEEE.

Donald M Hepburn received his B.A. (Hons) from the Open University in 1987 and the Ph.D. degree from Glasgow Caledonian University (GCU) in 1994. He is a Senior Lecturer at GCU, a member of the IEEE, Institute of Physics, the IET and C.Eng.

He has 20 years of industrial research experience and has been involved in research into HV insulation systems at GCU for over 20 years. His research interests cover monitoring physical and chemical change in HV/MV insulation materials and application of advanced digital signal processing to information from electrical, acoustic and RF monitoring techniques.